energies

MDPI

Article

Geopolymer Building Materials Based on Fly Ash in Terms of Removing SO_2, CO_2, and Water Vapor

Katarzyna Zarębska, Jakub Szczurowski *, Magdalena Gazda-Grzywacz, Wojciech Wróbel, Jakub Bator and Paweł Baran

Faculty of Energy and Fuels, AGH University of Krakow, al. Mickiewicza 30, 30-059 Krakow, Poland; zarebska@agh.edu.pl (K.Z.); magdago@agh.edu.pl (M.G.-G.); wwrobel@agh.edu.pl (W.W.); bator@agh.edu.pl (J.B.); baranp@agh.edu.pl (P.B.)

* Correspondence: szczurow@agh.edu.pl

Abstract: This paper presents the results of sorption tests against selected gaseous pollutants SO_2, CO_2 and H_2O on geopolymer materials obtained from high-calcium fly ash from lignite power generation. In the synthesis process, activation of geopolymer materials was carried out using KOH and NaOH. It was found that the activating agent significantly affects the porous structure of the samples. The sorption experiments conducted for the KOH-activated sample showed high SO_2 adsorption efficiency, almost ten times higher than against CO_2. The results demonstrate the possibility of utilizing fly ash obtained from the lignite energy processing sector for the synthesis of geopolymers with potential application of the materials as functional plastering compounds.

Keywords: geopolymers; sorption; vapor removal; fly ash; air pollution

check for updates

Citation: Zarębska, K.; Szczurowski, J.; Gazda-Grzywacz, M.; Wróbel, W.; Bator, J.; Baran, P. Geopolymer Building Materials Based on Fly Ash in Terms of Removing SO_2, CO_2, and Water Vapor. *Energies* **2023**, *16*, 5188. https://doi.org/10.3390/en16135188

Academic Editor: F. Pacheco Torgal

Received: 20 June 2023
Revised: 3 July 2023
Accepted: 4 July 2023
Published: 5 July 2023

Correction Statement: This article has been republished with a minor change. The change does not affect the scientific content of the article and further details are available within the backmatter of the website version of this article.

Copyright: © 2023 by the authors. Licensee MDPI, Basel, Switzerland. This article is an open access article distributed under the terms and conditions of the Creative Commons Attribution (CC BY) license (https://creativecommons.org/licenses/by/4.0/).

1. Introduction

Responsible and sustainable waste management, especially in the energy and chemical sectors of coal processing, is a critical element in ensuring efficient use of natural resources while minimizing negative impacts on the environment and human health [1]. Coal plays a significant role in meeting the world's energy needs, especially in countries whose energy economy is based on this resource. The process of generating electricity and heat from coal is burdened with the generation of a significant amount of fly ash. Global fly ash production in 2020 amounted to 7.575 Mt (China: 3.760 Mt; India: 760 Mt; Indonesia: 564 Mt; Australia: 493; USA: 485 Mt; Russia: 398 Mt; EU27: 301 Mt) [2,3]. In connection with the tightening of environmental regulations, particularly in the European Union (EU), concerning both emissions of pollutants and greenhouse gases [4], as well as the production and storage of combustion by-products (CBPs), it is important to develop a closed-loop economy model [5]. In Europe, about 85% of the produced ashes are mineral components that are suitable for reuse. The greatest potential for neutralizing and utilizing fly ash lies in the construction and building materials production sectors. Particularly promising is the possibility of its utilization as a component for the production of cement or new building elements (recycling). Polish power plants and combined heat and power plants produce approximately 20 Mt of CBPs from coal every year, including fly ash and slag [6]. Utilizing such waste also brings economic benefits, such as avoiding landfilling. In recent years, research on obtaining modern, environmentally acceptable materials using CBPs has gained popularity. These materials are known as geopolymers [7]. Geopolymers have become the subject of scientific research and industrial implementation in many countries, especially those with significant resources of synthesis precursors such as natural metakaolin (e.g., in Australia) or fly ash obtained in industrial and energy processes. Figure 1 shows the most commonly used substrates, primary and secondary, for the production of geopolymers.

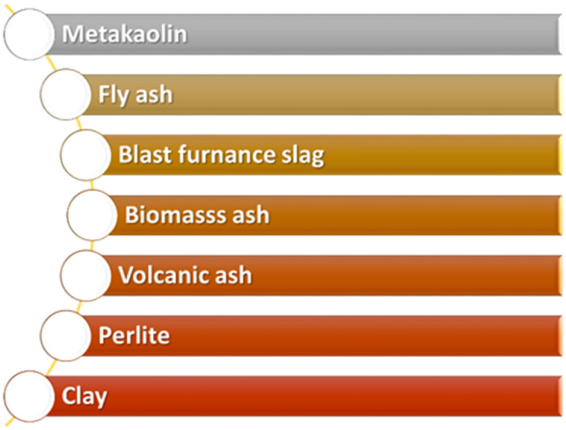


Figure 1. The most common precursors for geopolymer synthesis. Developed based on [7].

Geopolymer materials have stable chemical and thermal properties and use inexpensive and widely available raw materials in a simple synthesis process [8,9]. These materials consist of long chains (copolymers) of silicon and aluminum oxides, as well as metal cations that stabilize them, most commonly sodium, potassium or lithium, and bound water [10]. Geopolymer concrete is used in construction, and a number of studies have shown that this material will become one of the most promising, with unique structure and properties [11].

Recently, in addition to the precursors for geopolymer synthesis listed in Figure 1, there is emerging research on the use of phosphorus slag. Phosphorus slag (PS) is a by-product of the phosphate industry, containing very large amounts of glassy phase and small amounts of P_2O_5 [12]. Chemically, phosphorus slag is similar to blast furnace slag in containing large amounts of SiO_2 and CaO with small amounts of Al_2O_3 and P_2O_5. The use of PS as an additive to concrete has some limitations, as phosphorus oxide prolongs setting time and reduces strength, especially in the early stage. However, the addition of finely ground PS has a favorable effect on frost resistance properties compared to material with fly ash [13]. The authors also showed that the addition of ground PS has a stronger effect on pore fragmentation after 28 and180 days than the corresponding material with fly ash addition. The problem of low early strength has not been solved for the present moment, and elimination of the problem is seen in optimizing the slag dosage in combination with the selection of an appropriate activator and curing temperature [14]. In the case of geopolymer synthesis, the direct use of phosphoric slag yields low strength values due to its low aluminum oxide content. A study of geopolymer synthesis using PS and fly ash showed a significant change in the geopolymer obtained when the proportion of fly ash was 25% [15]. A 28% higher compressive strength was obtained. The addition of ash and increasing the amount of activator also reduced the porosity of the obtained geopolymer.

However, a detailed and in-depth review specifically addressing the high temperature exposure and fire resistance of fly-ash-based geopolymers is still lacking. The authors of paper [16] have comprehensively reviewed recent research on mix design, curing, and their effects on the thermal and fire resistance of F-grade fly-ash-based geopolymers. They discussed the influence of various alkalis on the synthesis process and their effect on thermal resistance. They also discussed the evolution of material properties during exposure to high temperatures and the key parameter of porosity, to avoid damage such as spalling. In the [17] study, the authors examined the effect of adding silica aerogel, which has super thermal insulation and excellent sound absorption. In the study, they used four types of silica aerogel with different particle sizes (2–40 μm, 100–700 μm, 100–1200 μm, 700–4000 μm). The results obtained show that larger silica aerogel particles are more beneficial for acoustic absorption and thermal insulation, while smaller aerogel particles are less effective for insulation properties. The optimal geopolymer foam aerogel (GFAR) obtained achieved a thermal conductivity of 0.133 W/(m·K), an average acoustic absorption coefficient of 0.51 at a density of 715.2 kg/m^3. The result of this study is necessary to explain

the use of larger silica aerogel particles in geopolymer foam, focusing on the low dosage of silica aerogel while exploiting its full benefits. Moisture transport plays a key role in determining various properties related to the durability of cement-based materials. In [18], the moisture uptake of low-calcium binders (geopolymer type) and calcium-rich alkali-activated binders was investigated and compared with that of Portland-cement-based binders. Analysis of the water vapor sorption isotherms (WVSI) and the results of the mercury porosimeter test (MIP) revealed two significantly different pore structures. The fly-ash-based geopolymer binders exhibited a highly porous structure, in which a large volume of mesopores coexisted with a considerable volume of macropores. In contrast, the alkali-activated slag-based binders had a very fine pore structure, with relatively few large macropores. The difference in pore structure between the fly-ash-based and slag-based binders resulted in increased pore blocking and cavitation in the mixed systems due to the addition of slag. Sorption kinetics analysis showed a significant effect of the presence of calcium in the matrix on permeability reduction. In work [19], the role of Ca availability in the geopolymerization of alkali-activated mixtures of ladle slag and class F fly ash was investigated. The results show that the product layer enveloping the slag particles largely regulates Ca diffusion in the environment and enables the development of two distinct gels, namely C-(N)-A-(S)-H and N-(C)-A-S-H. With 8% Na_2O, a dense matrix is obtained comprising a geopolymer gel and a Ca-enriched gel. Competition between the different reaction mechanisms of the two gels determines the initial properties and thermal performance of the hybrid binder. A thermal degradation model for a hybrid geopolymer comprising a geopolymer gel and a Ca-enriched gel is proposed to describe the effects of gel compatibility on the thermal behavior of the Ca-containing geopolymer.

Geopolymers also have other excellent practical applications—they are used as modern, inorganic porous materials. They can be used in environmental protection as sorbents for pollutants from water and wastewater or gases. The microstructure of geopolymers shows irregular pores with a larger specific surface area, and the three-dimensional network structure promotes the trapping of adsorbed substances [7]. Adsorption is the process of mass transfer. The process is used in many industrial technologies, and it is carried out using adsorbents [20,21]. Adsorption on geopolymers can be used for purification, decolorization, separation or detoxification [22]. Importantly, the use of geopolymers as building materials, especially those of waste origin such as fly ash, with adsorption properties, provides double benefits. First, we use waste to produce a modern adsorbing material, thus minimizing the amount of stored pollutants while simultaneously obtaining a substitute material. Second, this geopolymer is used as a modern material for the sorption or concentration of dispersed pollutants [23]. The development of research on economic, efficient and new ecological adsorbent materials is currently a developmental trend [24].

Common air pollutants emitted directly into the atmosphere due to industrial or energy production include sulfur dioxide, carbon monoxide, carbon dioxide, nitrogen oxides, and heavy metals. In 2021, according to the International Energy Agency (IEA), global CO_2 emissions rose by 6% to the highest level ever recorded at 36.3 billion tonnes [25]. The main culprits for this state of affairs are the industrial sectors, transportation, and non-renewable energy production. Adverse weather conditions and energy market conditions led to an increase in coal combustion despite the growth of energy production from renewable sources, as the demand for non-renewable energy revived in 2021 after the pandemic period. The increase in CO_2 content globally enhances the greenhouse effect worldwide, leading to global warming and other adverse phenomena such as sea-level rise [26]. Figure 2 presents global carbon dioxide emissions in the industrial sector.

In the first quarter of 2022, greenhouse gas emissions in the EU economy totaled 1.028 million tonnes of CO_2 equivalents, slightly below pre-COVID levels recorded in the first quarter of 2019 [27]. In Poland, CO_2 emissions in 2020 were estimated at around 303.52 million tonnes, which is 35.7% less compared to emissions in the base year (1988) and 4.7% less compared to 2019. CO_2 emissions accounted for 80.7% of total greenhouse gas emissions in Poland in 2020 [28].

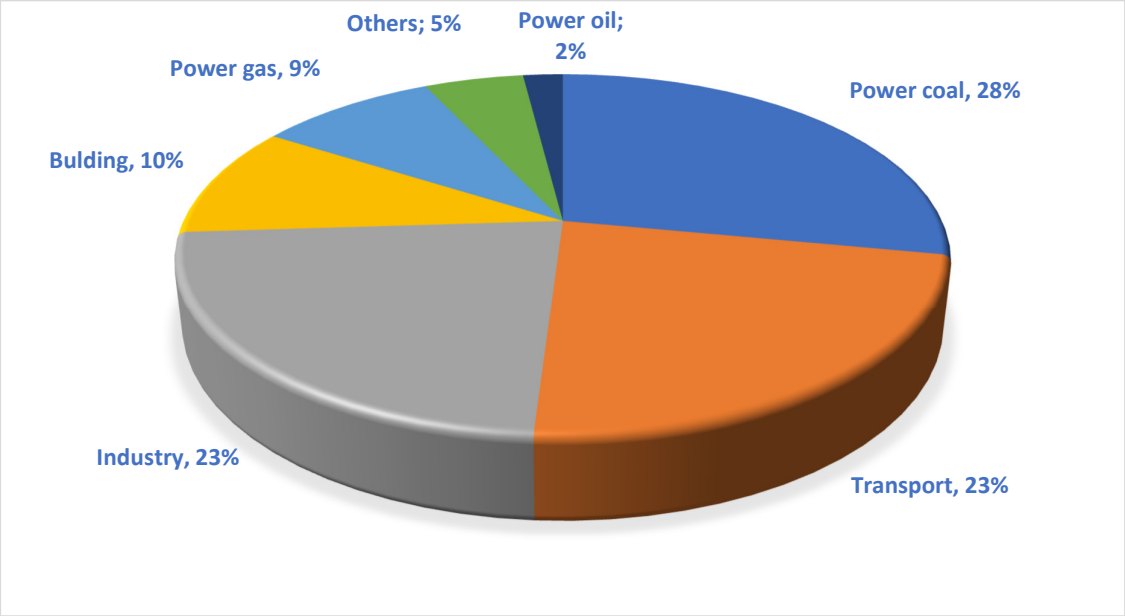


Figure 2. The structure of global CO_2 emissions (36.3 billion tons) with a breakdown of the sector of origin. Developed based on [18].

Atmospheric emissions of sulfur dioxide (SO_2) are a concern due to their adverse impact on climate and human health [29]. Inhaling SO_2 increases the risk of diseases such as stroke, heart disease and lung cancer. Sulfur oxides (SO_x) can react with other compounds present in the atmosphere to form sulfur aerosols, and by reacting with water they form sulfuric acid, the main component of acid rain, which causes soil and water acidification and damages the leaves and growth cones of plants, limiting photosynthesis [30]. SO_2 emissions mainly come from the consumption of fossil fuels, especially for electricity generation, and from industrial activities such as oil refining or metal smelting [31]. The global emissions of this gas in 2020 were recorded at 41.93 kt, of which 14.97 came from coal combustion, 8.85 from oil and gas combustion, 4.88 from smelting, and 13.23 kt from volcanic eruptions. This proves that over 68% of sulfur dioxide emissions come from anthropogenic sources [32]. Figure 3 shows global SO_2 emissions by sector.

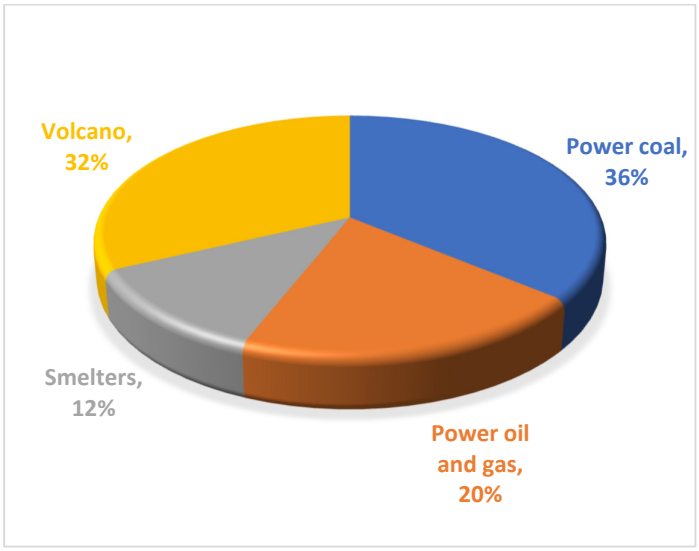


Figure 3. The structure of global SO_2 emissions (41.93 kt) with a breakdown by sector of origin. Developed based on [25].

In 2019, all EU member states adhered to their sulfur dioxide (SO_2) emission ceilings. Poland was the largest emitter, followed by Germany and Spain. SO_2 emissions in the EU have decreased by 77% since 2005. In 2018–2019, almost all member states (24 out of 27) reported emission reductions, resulting in an overall 11% reduction for the entire EU. Sulfur dioxide is a pollutant subject to emission limits defined in Directive 2001/81/EC [33]. According to this directive, by 2010, Poland was to limit its annual SO_2 emissions to no more than 1397 Gg. This limit was met during the period of 2010–2018. Under the current directive 2016/2284, Poland should achieve a 59% reduction in SO_2 levels compared to 2005 by 2020. In 2018, the reduction in this pollutant's levels relative to 2005 was 56%.

This study deals with the issues of the prospective use of geopolymers as alternative, cost-competitive and environmentally friendly adsorbents. The study investigated the sorption properties of geopolymers synthesized based on fly ashes from brown coal energy combustion—most of this raw material in the EU is used for electricity production. The consumption of brown coal in the EU in 2020 amounted to 246 million tonnes.

The assumptions and procedures made in this paper are in line with the "circular economy" method. Sorption studies were conducted with respect to the sorbates of SO_2, CO_2, and water vapor. The issues of the first two pollutants are common and have been discussed above, while water vapor itself cannot be considered a pollutant. However, regardless of the requirements imposed on the geopolymer materials themselves, there are also a number of requirements that must be met by a building component made of geopolymer concretes. Modern building materials must not only have proper load-bearing capacity or strength, but also elevated thermal insulation. In the event of significant moisture in structural elements, both strength parameters and thermal insulation can be reduced. This applies especially to highly porous building materials, such as geopolymer concrete. Its numerous pores promote the introduction of environmental water into the interior of structural elements in significant amounts. The presence of water, on the one hand, can significantly reduce the mechanical parameters of the material, and on the other hand, can worsen its thermal conductivity [34], leading to a significant increase in heat loss through a moist element. This article presents research aimed at analyzing the behavior of geopolymer concrete in contact with water vapor.

The purpose of this work was to conduct sorption tests for geopolymer materials obtained at an earlier stage of work, synthesized from fly ash from lignite combustion. Two of the 10 synthesized materials with the best mechanical, thermal and refractory properties were selected for sorption tests. The previously mentioned vapors SO_2, CO_2 and H_2O were used as sorbates. The tests made it possible to determine the ability of geopolymer blocks to adsorb selected gaseous pollutants. They were aimed at verifying whether the material, obtained from fly ash, can find application in accordance with the principles of a closed-loop economy, as a material that reduces the amount of CO_2, SO_2 and H_2O in atmosphere air.

2. Materials and Methods

2.1. Substrates

The authors of this study conducted previous research on the synthesis of geopolymers based on fly ash from brown coal energy combustion to investigate the insulation properties of the obtained materials in [35]. In the study, fly ash from lignite combustion was used. The oxide composition of fly ash used for the ash syntheses was determined using an Epsilon 3 ED-XRF spectrometer from PANalytical. Oxide content (Mass content, (%)) of fly ash: Na_2O 0.01, MgO 1.34, Al_2O_3 19.67, SiO_2 42.25, P_2O_5 0.12, SO_2 2.00, K_2O 0.15 CaO 19.50, TiO_2 1.54, MnO 0.03, Fe_2O_3 4.60, LOI 3.70, Free CaO 2.80. The selected expanded perlite is EP 150 (Class 1). Its chemical composition includes the following compounds: SiO_2 (65–73%), Al_2O_3 (10–18%), K_2O + Na_2O (6–9%), CaO (2–6%) and Fe (1–2%).

For the purposes of these sorption analyses, two materials that showed the best strength properties in the [35] study for the assumed goals were selected: GeoK and GeoNa.

The properties of fly ashes are determined by many factors, the most important of which include: the type of coal burned; the type of installation in which coal combustion occurs, i.e., boiler type and technological conditions of combustion; fuel preparation method; method of capturing, removing and storing ashes; gas desulfurization technology; and the type of SO_2 sorbent used (if gas desulfurization processes are carried out simultaneously).

2.2. Synthesis

The adopted methodology for sample synthesis involved mixing the substrates, 5-min stabilization in a shaker, pouring the samples into a special standardized mold, and curing at a temperature of 308 K. Two series of experiments (i) and (ii) were planned and carried out for GeoK and GeoNa, respectively. Liquid components were introduced into the vessel at room temperature, and solid substances were gradually added while stirring with a glass stirrer to obtain a homogeneous, liquid mixture. The synthesis of geopolymers was preceded by the preparation of synthesis mixtures.

The first set, designated GeoK, involved synthesis using the following liquid components: 8 mol/dm^3 of KOH solution and potassium water glass in a weight ratio of 1:2, and solid components: a mixture of expanded perlite and fly ash in a weight ratio of 1:1.

The second batch, designated GeoNa, was made identically except for the replacement of KOH with an 8 mol solution of NaOH.

The mixture was then placed in a shaker for 5 min to stabilize the sample volume, which was then placed in the mold. The materials were placed in an oven heated to a temperature of 308 K for 24 h. Mixing, compaction, and heating processes for the GeoK series were carried out in the same way as for the GeoNa series, described in detail in [28].

2.3. Measurement Methods

2.3.1. Porosimetry

The porosity of materials is one of the key factors affecting their physical and chemical properties, such as density, specific surface area, chemical reactivity and moisture adsorption capacity. The PASCAL porosimeter—an advanced laboratory tool for measuring the porous structure of materials—was used for these porosity studies. The instrument operates on an invasive principle, which means that the flow of fluid through the porous structure of the material is measured directly. During the measurement, a sample of the material is filled with a fluid (in this study, with mercury) and then subjected to various pressures. Based on the measured volume of fluid flowing out of the sample at different pressure values, the size and distribution of pores in the material being studied can be determined. The results of porosimetric analysis allow us to obtain TCV—Total Cumulative Volume—the total volume of pores, porosity in percent, bulk density and apparent density for 101.3 kPa and 150 MPa, volume of pores with a diameter below 5 nm, and the mean pore diameter size.

2.3.2. Microscopy

Microscopic images were obtained using the VHX-7000 digital optical microscope from the KEYENCE America series. The specialized design with high-resolution lenses, a 4 K CMOS sensor and lighting technology was used to create an optical shadow effect. Scanning electron microscopy (SEM) was performed using the JOEL JSM-7500F microscope with an EDS attachment.

2.3.3. Textural Properties

The porous texture of all samples was investigated using N_2 adsorption/desorption isotherm at 77 K with a static volumetric analyzer, Autosorb-1-C (Anton Paar Quantachrome Instruments, Boynton Beach, FL, USA). Before the gas sorption experiments, all samples were degassed at 473 K for 6 h under vacuum. The amount adsorbed at each point p/p_0 (relative pressure) determines the adsorption isotherm. Using the N_2 adsorption isotherms at 77 K, the specific surface area was calculated using the Brunauer–Emmett–

Teller (BET) theory [36], with the appropriate fitting approach for microporous adsorbents described by Rouquerol et al. [37]. The volume and surface area of the micropores were calculated using the Dubinin–Radushkevich (DR) equation. The Barrett–Joyner–Halenda (BJH) method [38,39] using the Kelvin model for pore filling was used to calculate the volume and surface area of the mesopores. The total pore volume was obtained from the amount of N_2 adsorbed at a relative pressure close to unity ($p/p_0 = 0.995$), assuming that the pores were filled with liquid adsorbate at that point.

2.3.4. Sorptions of CO_2, SO_2 and H_2O

The sorption studies of CO_2 for the test samples were performed using Autosorb®-1-C Chemisorption—Physisorption Analyzer (Anton Paar GmbH, Graz, Austria). Before performing gas sorption experiments, the samples were freed from contaminants such as water by degassing under a vacuum at a temperature of 473 K for 6 h. Once clean, the sample was brought to a constant temperature by means of an external bath. The CO_2 sorption isotherms were obtained at 298 K and up to a pressure of 1 bar. The SO_2 sorption test was carried out at a temperature of 298 K using an apparatus equipped with a Sartorius sorption microbalance. The experiment focused on measuring the increase in sample mass with the increase in SO_2 pressure. The pressure was increased at regular time intervals, allowing for the saturation of the sample at each stage of the test. The sorption was carried out in three cycles, including the sorption and desorption process on the same geopolymer. Desorption was carried out by reducing the pressure to 10^{-2} Pa. The cyclic adsorption-desorption experiments aimed to investigate the possibility of regenerating the analyzed material. H_2O sorption isotherms were determined by volumetric technique using liquid micro burettes at a temperature of 303 K. This technique allows for the determination of adsorption and desorption isotherms of polar substances such as water or alcohols, as well as non-polar compounds, such as benzene, across the entire range of relative pressures, i.e., from absolute vacuum to the equilibrium vapor pressure.

2.4. Research Results

The obtained materials (Figure 4) were characterized by their apparent and true density, porosity (%), pore volume in two ranges, specific surface area, microscopic analysis, SEM morphological analysis, surface chemical composition by EDS, thermal conductivity, ordinary refractoriness, compressive strength, and finally by the sorption of SO_2, CO_2, and H_2O vapors.

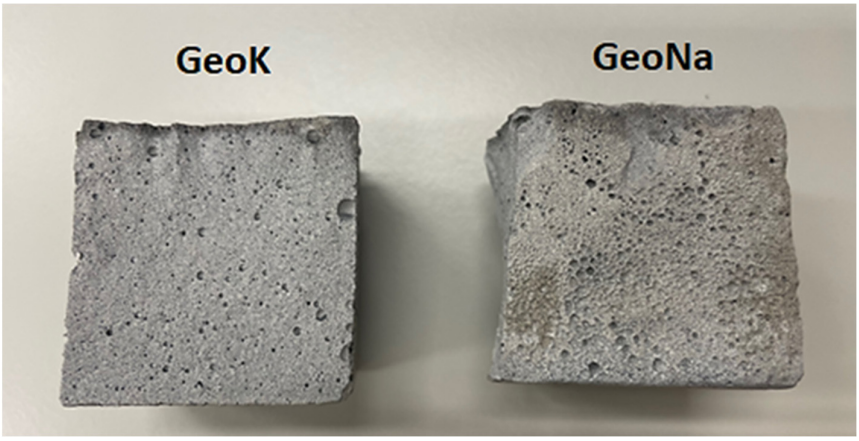


Figure 4. The obtained geopolymers materials.

In Figures 5 and 6, macroscopic images of the geopolymers GeoK (Figure 5) and GeoNa (Figure 6) are presented, respectively. The images were taken using a Keyence International microscope (Mechelen, Belgium) NV/SA Global Support. No significant

morphological differences were found between the materials. Later SEM and porosity analyses showed the presence of macropores.

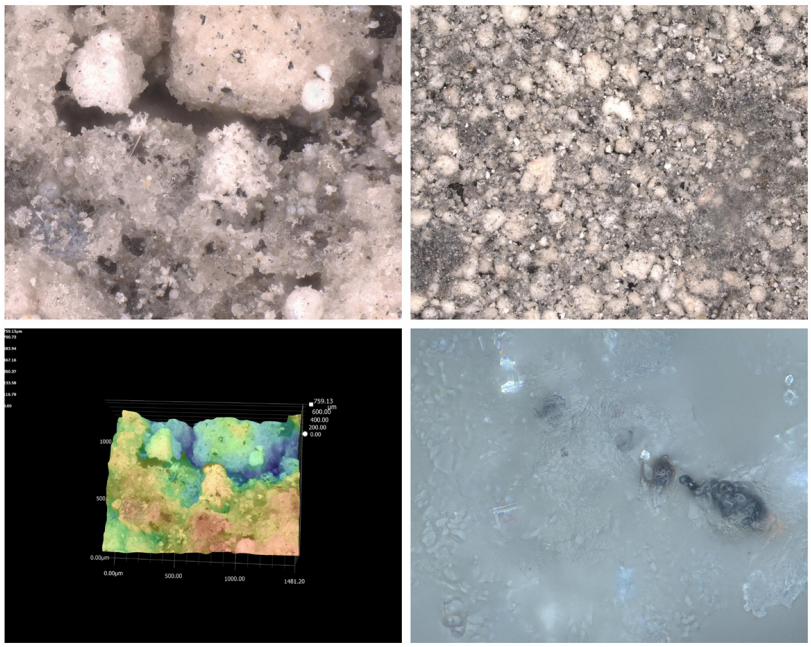


Figure 5. Microphotographs of the GeoK material.

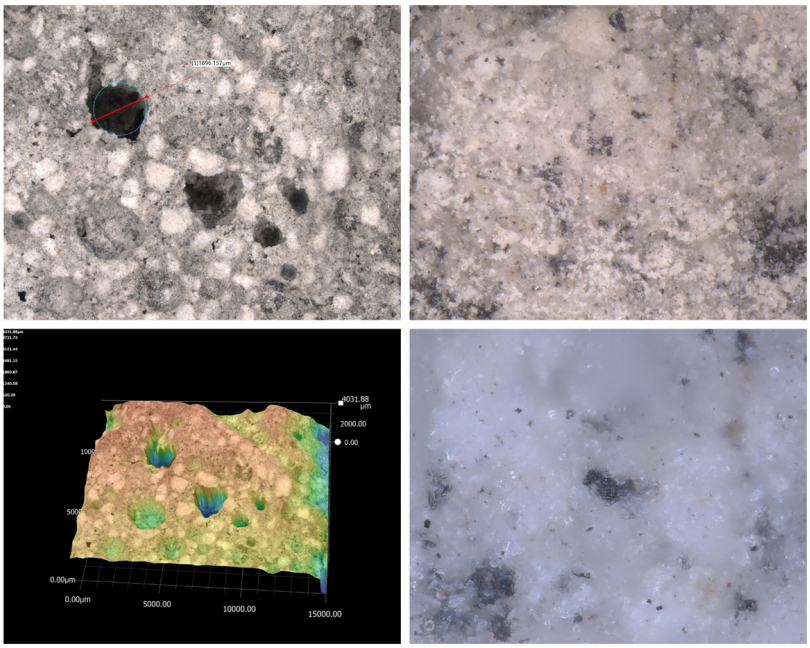


Figure 6. Microphotographs of the GeoNa material.

In the SEM images (Figures 7 and 8), representative microstructures of the investigated geopolymer materials based on brown-coal fly ash are presented. The chemical composition is uniform in the analyzed areas for both GeoK and GeoNa geopolymers, mainly consisting of oxygen, silicon, aluminum and potassium. The images show voids from air bubbles formed during the mixing of the geopolymeric mass, and a few crystalline phases in the form of inclusions. On the surfaces of the geopolymer materials obtained from brown coal fly ash, no undissolved ash particles are observed.

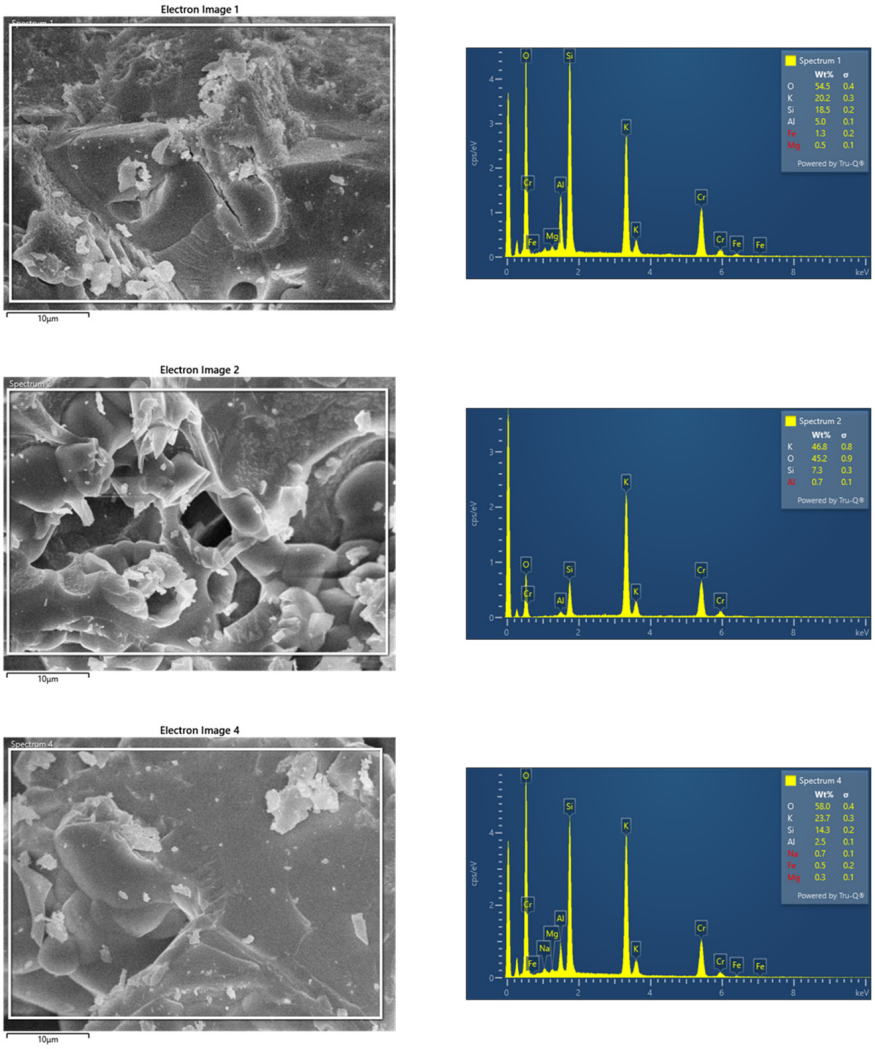


Figure 7. SEM images and EDS chemical composition analysis of GeoK.

In Table 1, the textural parameters of the investigated geopolymers, GeoK and GeoNa, are presented. The following parameters were determined:

- SSA_{BET}, [m^2/g]—Specific Surface Area by Brunauer–Emmett–Teller (BET);
- V_{DR}, [cm^3/g]—Volume of micropores from Dubinin–Radushkevich equation;
- S_{DR}, [m^2/g]—Surface area of micropores from Dubinin–Radushkevich equation;
- V_{BJH}, [cm^3/g]—Volume of mesopores from Barrett–Joyner–Halenda (BJH) analysis;
- S_{BJH}, [m^2/g]—Surface area of mesopores Barrett–Joyner–Halenda (BJH) analysis;
- V_{total}, [cm^3/g]—Total pore volume calculated at $p/p_0 = 0.995$.

Table 1. Parameters characterizing the porous structure of the investigated samples, which were determined based on low-temperature nitrogen (77 K) adsorption.

Sample	SSA_{BET} (m^2/g)	S_{DR} (m^2/g)	V_{DR} (cm^3/g)	S_{BJH} (m^2/g)	V_{BJH} (cm^3/g)	V_{Total} (cm^3/g)
GeoK	10.1	9.2	0.003	8.7	0.058	0.081
GeoNa	3.5	3.1	0.001	3.3	0.024	0.035

In Table 2 and in Figures 9–11, the results of mercury porosimetry tests for the GeoK and GeoNa materials are presented.

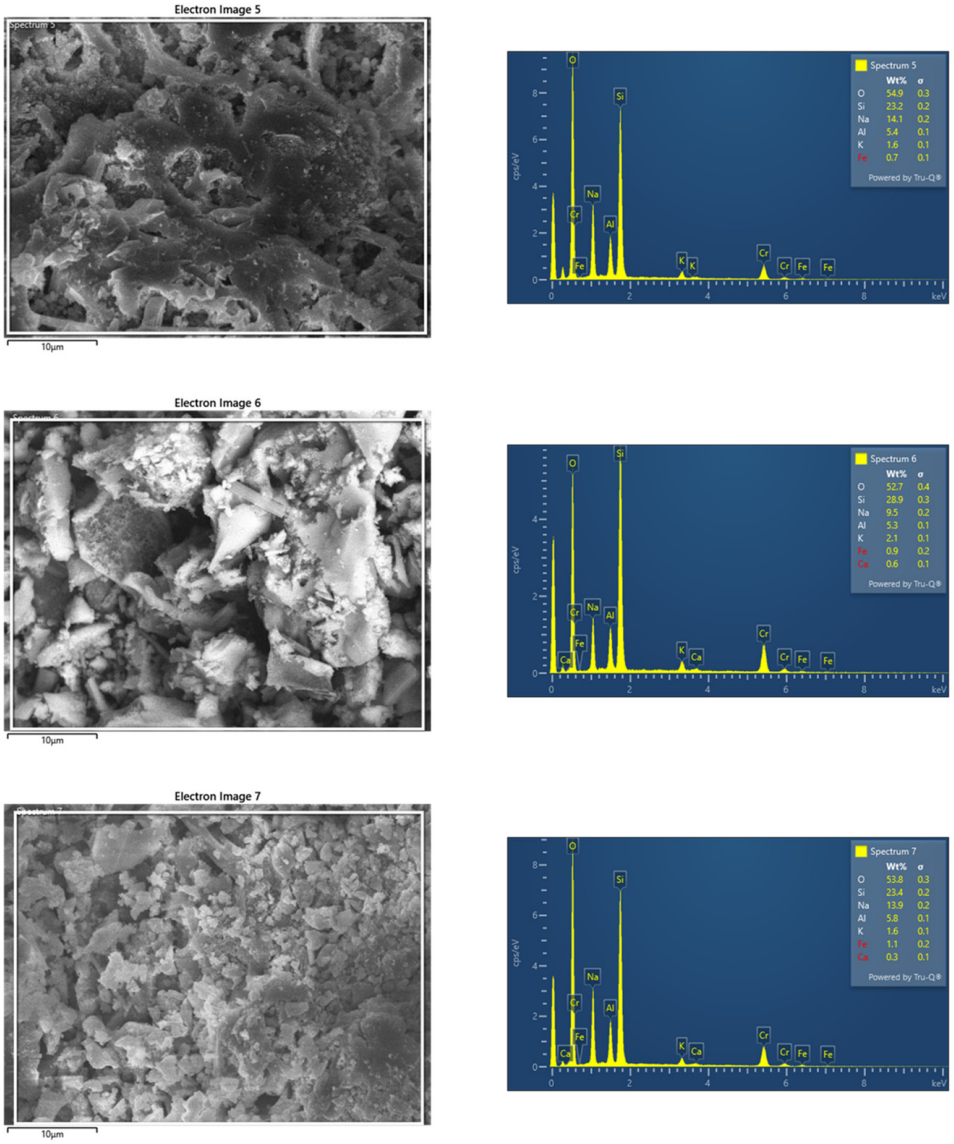


Figure 8. SEM images and EDS chemical composition analysis of GeoNa.

Table 2. Results of porosimetry tests.

Quantity	GeoK	GeoNa
Total cumulative volume, TCV (mm^3/g)	129.2	387.1
Porosity (%)	21.23	42.97
Density, bulk density ($g/cm^{3)}$	1.1441	0.9914
Density, apparent density, 101.3 kPa ($g/cm^{3)}$	1.5952	1.0910
Density, apparent density, 150 MPa (g/cm^3)	2.0867	1.9465
Pore volume < 5 nm	0.1009	0.1153
Average pore radius (nm)	7.0	90.6

In Figures 12–14, the IR spectra of obtained geopolymer materials based on lignite fly ash are presented.

In Figure 15, XRD spectra for obtained geopolymer GeoK and GeoNa are presented.

On Figures 16–18, the sorption isotherms of materials GeoK and GeoNa are presented for CO_2, SO_2 and water vapor, respectively.

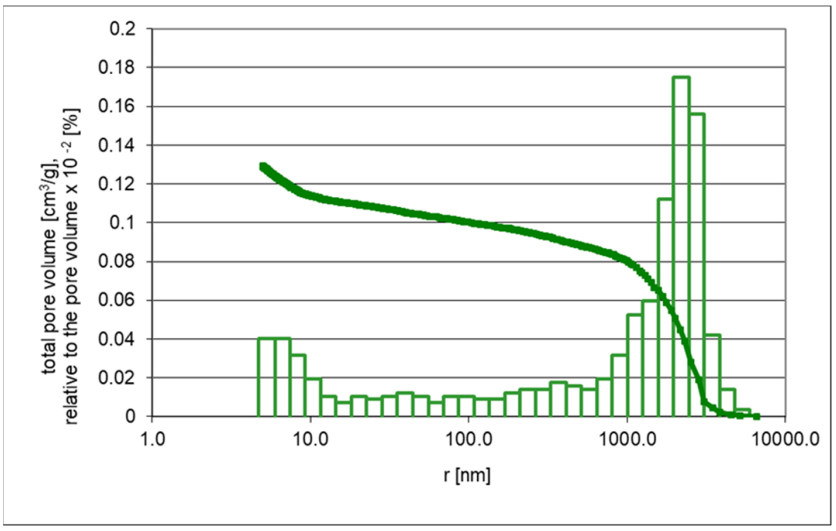


Figure 9. Histogram with TCV for material GeoK.

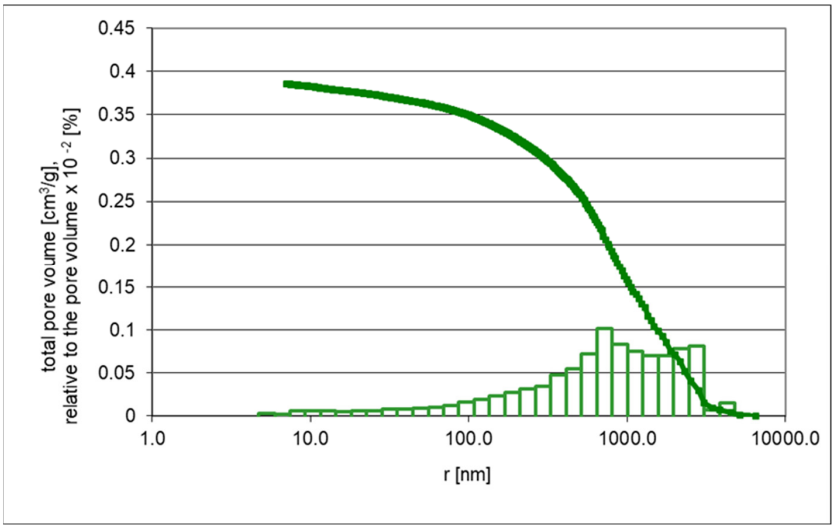


Figure 10. Histogram with TCV for material GeoNa.

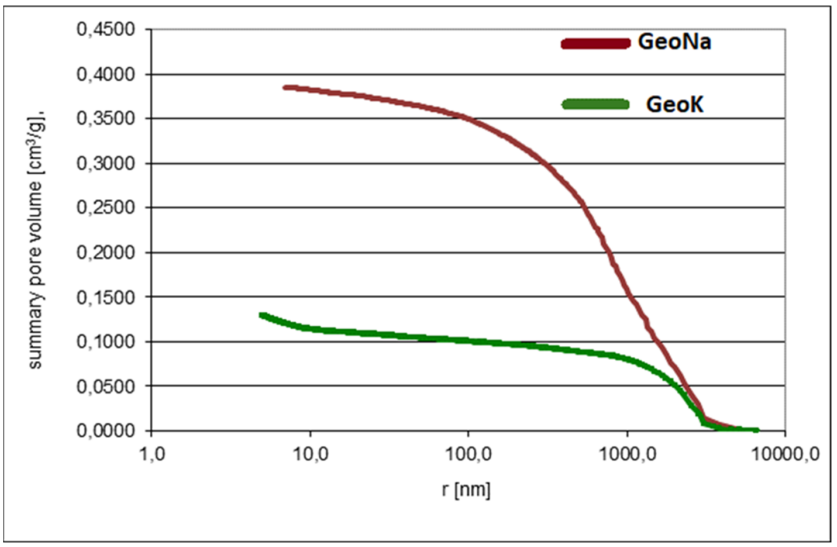


Figure 11. Histogram with TCV for materials GeoK and GeoNa.

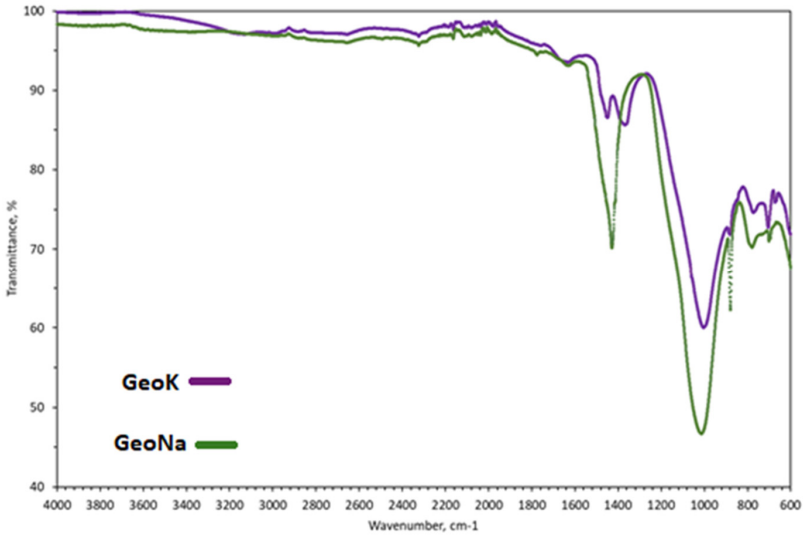


Figure 12. Infrared spectra for GeoK and GeoNa geopolymers before SO_2 sorption.

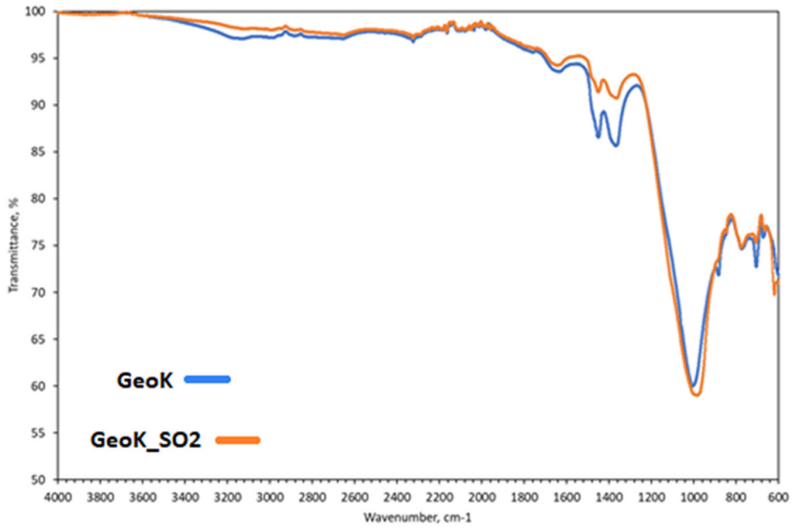


Figure 13. Infrared spectra of the GeoK geopolymer before and after SO_2 sorption.

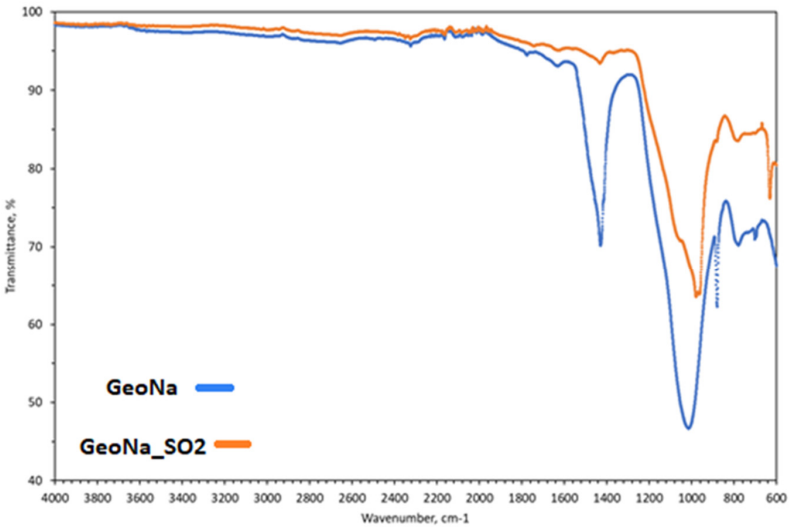


Figure 14. Infrared spectra of the GeoNa geopolymer before and after SO_2 sorption.

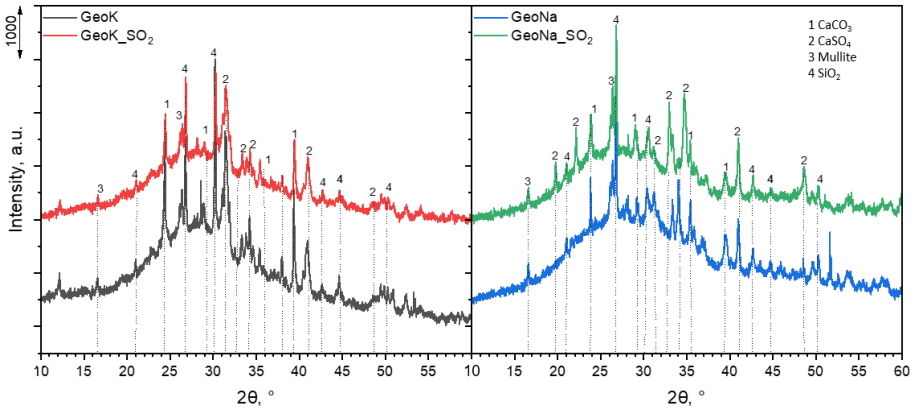


Figure 15. XRD spectra before and after SO_2 sorption for geopolymer GeoK (left) and GeoNa (right).

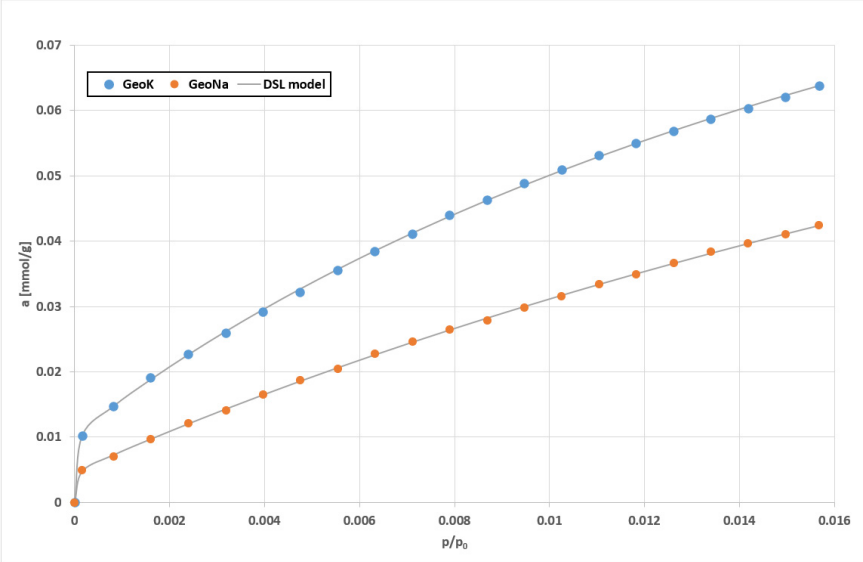


Figure 16. Isotherm of CO_2 sorption for geopolymer GeoK and GeoNa (circle—experimental points, line—Langmuir model fitting).

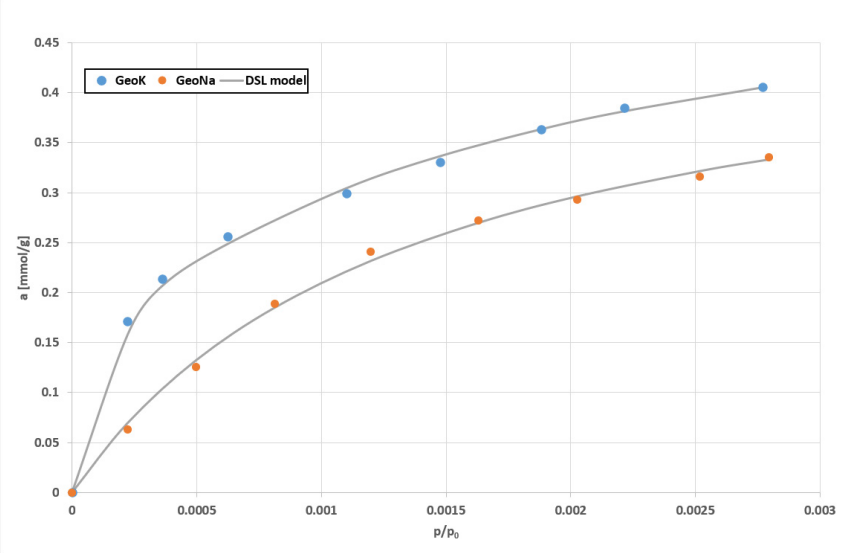


Figure 17. Isotherm of SO_2 sorption for geopolymer GeoK and GeoNa (circle—experimental points, line—dual-site Langmuir model fitting).

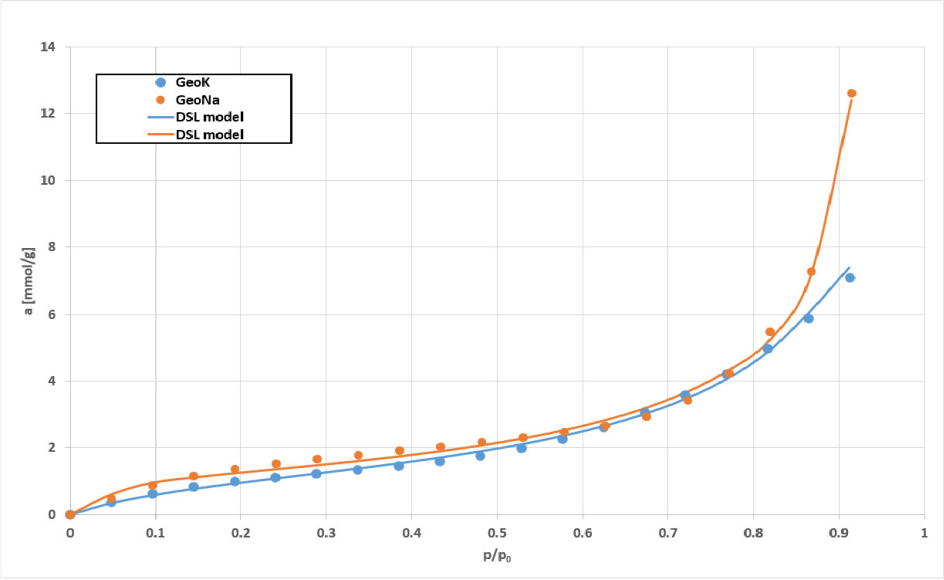


Figure 18. Isotherm of H_2O vapor sorption for geopolymers GeoK and GeoNa (circle—experimental points, line—GAB model fitting).

The sorption studies conducted on selected geopolymeric samples with respect to carbon dioxide, sulfur dioxide and water vapor showed a close relationship with the structure of the tested samples. In the case of sample GeoK, we observe a higher sorption capacity for CO_2 and SO_2, resulting from a larger specific surface area and a higher proportion of smaller pores in the sample structure (Table 2) compared to sample GeoNa. The isotherms for these sorbates are similar in shape to Type I isotherms according to IUPAC, indicating that the adsorption occurs in pores with the smallest range. It should also be noted that the sorption capacity, in the context of a low specific surface area, is relatively high, and for SO_2 it is only slightly lower than for materials with significantly higher specific surface area.

3. Discussion

The obtained materials were characterized in terms of apparent and true density, porosity (%), pore volume in two ranges, specific surface area, microscopic analysis, SEM morphological analysis, surface chemical composition by EDS, thermal conductivity, ordinary flame resistance, compressive strength (see Table 3), and finally by sorption of SO_2, CO_2 and H_2O. Figures 5 and 6 present macroscopic images of GeoK and GeoNa geopolymers. SEM (Figures 7 and 8) and porosity analyses showed the presence of macropores.

Table 3. The properties of the obtained materials from the GeoK and GeoNa series based on [35].

Quantity	GeoK	GeoNa
Compressive strength, MPa	4.901	4.984
Refractoriness, °C	1200	1000
Thermal conduction coefficient, W/m·K	0.207	0.232

The macroscopic image of the samples, as seen in Figure 4 and in the microphotographs (Figures 5 and 6), is similar. The distribution of material that has geopolymerized is relatively homogeneous. Some voids are noticeable, as seen in Figure 4. The GeoNa sample has slightly more of these voids. This is observed both in the macroscopic image and in the magnifications of the microphotographs. These spaces will largely account for the porosity of the sample. In contrast, these images will not be useful for evaluating samples for their sorption properties.

The SEM images show representative microstructures of the studied geopolymer materials. The chemical composition is homogeneous in the analyzed areas for both GeoK

and GeoNa geopolymers, consisting mainly of oxygen, silicon, aluminum and potassium. The images show voids from air bubbles formed during mixing of the geopolymer mass and a few crystalline phases in the form of inclusions. No undissolved ash particles were observed on the surface of the materials. The studied geopolymers have different pore distributions with varying sizes and structures. The porosimetry results are shown in Figure 9, Figure 10, and Figure 11. The histogram results show significant variation between the two samples. Figure 9 shows the results for the GeoK sample. The pore distribution is bimodal, with a significant proportion of pores in the range below 10 nm and a significant proportion in the pore range above 1000 nm to 6000 nm. The histogram obtained for the GeoNa sample (Figure 10) shows that this sample has a quite different pore structure. This sample has a wide range of pore contribution in the range from 50 to 6000 nm. The differences indicated for the two samples will have important consequences in the adsorption properties. Because if we look at the total pore volume, the GeoNa sample has more than twice the total pore volume compared to the GeoK sample. Sample GeoNa also has twice the porosity (Table 2). However, it should be taken into account that in the case of sorption phenomena, it is not the porosity itself, or the total pore volume, that is relevant, but the pore size. The adsorption phenomenon will only take place in mesopores (pores in the range of 2–50 nm according to IUPAC) and micropores (<2 nm). Macropores are not the part of the adsorbent where adsorption occurs. These pores mainly have a transport role for the sorbate. The average pore size (Table 2) shows that the GeoK sample has an average pore size of 7 nm (i.e., it is in the mesopore range according to the IUPAC classification), while the GeoNa sample shows a value of 90 nm (macro pore range).

Pore surface area and structure have a significant effect on the ability of a geopolymer to adsorb gases and liquids. The larger the pore surface area, the greater the surface area available for adsorption. GeoK has a higher proportion of pores in the micro and meso range (Table 2, Figure 9) compared to the total pore volume, and these pores play a decisive role in the adsorption phenomenon, resulting in increased sorption for CO_2 and SO_2 adsorbates. On the other hand, the GeoNa sample, despite its high total pore volume and twice the total porosity compared to the GeoK sample, is a sample with a dominant share of macropores (Table 2) because the average pore size is 90 nm. In contrast, the histogram (Figures 16 and 17) confirms that the proportion of micropores is negligible. Hence, the lower values of sorption adsorption towards CO_2 and SO_2.

Experimental CO_2 adsorption sites show typical type I adsorption behavior, according to the IUPAC classification (Sing et al., 1988); CO_2 adsorption isotherms on investigated geopolymer materials cannot be accurately described by a simple Langmuir model, and the dual-site Langmuir approach, shown in Figure 16, proved to be the most effective and appropriate correlation able to describe the experimental behavior over the entire pressure range. Likewise, the dual-site Langmuir model was applied to the SO_2 adsorption experimental points (Figure 17).

The Langmuir theory proposes that adsorption occurs on specific sites on a surface until all sites are occupied. It originated from a kinetic model of gas adsorption and is based on a set of assumptions [40]. The assumptions of the Langmuir theory are as follows: All sites on the surface are identical and have an equal chance of being occupied. Each adsorbate molecule can occupy only one adsorption site. There are no interactions between the adsorbed molecules. The rates of adsorption and desorption are proportional to the number of available sites and the number of occupied sites, respectively. Adsorption is considered complete when all sites are filled. By employing these assumptions, rates for adsorption and desorption can be defined. The rate of adsorption is determined by the number of available surface sites and the pressure, which represents the number of gas molecules. It is also useful to define the fractional surface coverage, denoted as θ, which represents the ratio of occupied sites to the total number of sites. At equilibrium, the rate of adsorption is equal to the rate of desorption. Mathematically, it can be expressed as:

$$n(p) = n_m \frac{Kp}{1 + Kp} \quad (1)$$

n_m—is the moles adsorber at the completion of the monolayer, the maximum possible loading, K—the Langmuir constant exponentially related to the energy of adsorption, p—partial pressure.

An extension of the Langmuir model is to consider the experimental isotherm as the sum of several Langmuir-type isotherms with different capacities and affinities of the monolayer. It is assumed that the adsorbent presents several different types of homogeneous adsorption sites and that separate Langmuir equations should be applied to each of them. This is particularly applicable in cases where the structure of the adsorbent suggests the presence of different types of sites, such as crystalline materials with variable chemical compositions such as zeolites, MOFs and geopolymers. The resulting dual-site Langmuir adsorption isotherm model is:

$$n(p) = n_{m1}\frac{K_1 p}{1 + K_1 p} + n_{m2}\frac{K_2 p}{1 + K_2 p} \quad (2)$$

For both GeoK and GeoNa materials, sorption adsorption values were found to be 10 times higher against SO_2 than against CO_2, in the same relative pressure range. The differences in sorption adsorption of the tested sorbates are a result of the geometry of the two molecules. An SO_2 molecule with an angular structure and a relatively high dipole moment (1.60 D) interacts much better with the surface of the tested materials than a linear CO_2 molecule with zero dipole moment. A water molecule is characterized by an even higher polarization and a higher value of dipole moment (1.84 D).

The adsorption isotherms of water vapor in this particular case can be regarded as describing the relationship between the ambient relative humidity and the retained moisture in the material at constant temperature.

The Guggenheim–Anderson–de Boer (GAB) model is widely utilized to analyze adsorption isotherms of water vapors across various materials [41–44]. It consists of two components that are combined, with the first component describing the classical monomolecular layer expression found in Langmuir's adsorption isotherms, and the second component representing multilayer adsorption based on Raoult's law. According to this model, the sorbate molecules in the second layer possess the same characteristics as those in the upper layers but differ from those in the liquid state. The GAB model effectively characterizes sorption behavior over a broad range of relative pressures.

The expression for the Guggenheim–Anderson–de Boer (GAB) model is as follows:

$$n(p) = n_m\frac{CKp}{(1 - Kp)(1 - Kp + CKp)} \quad (3)$$

where: n_m is the monolayer capacity, p is pressure, C is the kinetic constant related to the sorption in the first layer, K is the kinetic constant related to multilayer sorption. C and K are the adsorption constants considering the different enthalpy of adsorption of the adsorbed phase compared to the enthalpy of condensation of the bulk phase.

The high sorptive capacity of the obtained materials with respect to water vapor determines their applicability for the regulation of indoor humidity, with high efficiency of SO_2 elimination, which makes the obtained materials potential sorbents towards these pollutants. GeoK and GeoNa samples, compared to SO_2 and H_2O, show significantly lower efficiency in terms of CO_2 adsorption.

4. Conclusions

Using various research methods, we investigated geopolymers obtained based on fly ash. The research presented in the article showed that the obtained geopolymers (GeoNa and GeoK) could adsorb certain amounts of CO_2, as well as significant amounts of sulfur dioxide (SO_2) and water vapor. The value of gas adsorption depended on the textural parameters of the synthesized materials and the type (chemical nature) of the sorbate (polarity and dipole moment). The activating agent used in the synthesis of geopolymers

(KOH or NaOH) significantly affects the obtained pore structure and, consequently, the adsorption properties of the materials.

The mechanical strength of the obtained samples does not predispose these materials to be used as a substitute for concrete in the construction industry, while the obtained properties such as sorptive adsorption towards the selected vapors and refractoriness provide opportunities for use as functional plastering compounds, allowing the management of waste in the form of fly ash from lignite coals and the removal of gaseous pollutants from the premises.

Author Contributions: Conceptualization, K.Z. and J.S.; methodology, K.Z.; software, J.S., P.B. and W.W.; validation, K.Z., P.B. and J.S.; formal analysis, K.Z., J.B. and W.W.; investigation, P.B., J.S.; W.W. and J.B. resources, P.B. and J.S.; data curation, M.G.-G.; writing—original draft preparation, M.G.-G., K.Z., J.S. and P.B.; writing—review and editing, K.Z., P.B., J.S. and M.G.-G.; visualization, J.S. and M.G.-G.; supervision, K.Z.; project administration, K.Z.; funding acquisition, K.Z. All authors have read and agreed to the published version of the manuscript.

Funding: This project was carried out within OPUS 2022. This research was fully funded by the National Science Centre, Poland, grant number OPUS-22 UMO-2021/43/B/ST8/01636.

Conflicts of Interest: The authors declare no conflict of interest.

References

1. Kowalska, N.; Brodawka, E.; Smoliński, A.; Zarębska, K. The European Education Initiative as a Mitigation Mechanism for Energy Transition. *Energies* **2022**, *15*, 6633. [CrossRef]
2. Coal-Fired Electricity–Analysis. Available online: https://www.iea.org/reports/coal-fired-electricity (accessed on 7 October 2022).
3. Ćwik, A.; Casanova, I.; Rausis, K.; Zarębska, K. Utilization of High-Calcium Fly Ashes through Mineral Carbonation: The Cases for Greece, Poland and Spain. *J. CO2 Util.* **2019**, *32*, 155–162. [CrossRef]
4. EU Best Available Techniques Reference Documents (BREFs)—European Environment Agency. Available online: https://www.eea.europa.eu/themes/air/links/guidance-and-tools/eu-best-available-technology-reference (accessed on 31 January 2023).
5. Sauvé, S.; Bernard, S.; Sloan, P. Environmental Sciences, Sustainable Development and Circular Economy: Alternative Concepts for Trans-Disciplinary Research. *Environ. Dev.* **2016**, *17*, 48–56. [CrossRef]
6. Czuma, N.; Samojeden, B.; Zarębska, K.; Motak, M.; Da Costa, P. Modified Fly Ash, a Waste Material from the Energy Industry, as a Catalyst for the CO_2 Reduction to Methane. *Energy* **2022**, *243*, 122718. [CrossRef]
7. Xu, J.; Li, M.; Zhao, D.; Zhong, G.; Sun, Y.; Hu, X.; Sun, J.; Li, X.; Zhu, W.; Li, M.; et al. Research and Application Progress of Geopolymers in Adsorption: A Review. *Nanomaterials* **2022**, *12*, 3002. [CrossRef] [PubMed]
8. Amran, M.; Debbarma, S.; Ozbakkaloglu, T. Fly Ash-Based Eco-Friendly Geopolymer Concrete: A Critical Review of the Long-Term Durability Properties. *Constr. Build. Mater.* **2021**, *270*, 121857. [CrossRef]
9. Luhar, S.; Nicolaides, D.; Luhar, I. Fire Resistance Behaviour of Geopolymer Concrete: An Overview. *Buildings* **2021**, *11*, 82. [CrossRef]
10. Kumar, S.; Kumar, R. Mechanical Activation of Fly Ash: Effect on Reaction, Structure and Properties of Resulting Geopolymer. *Ceram. Int.* **2011**, *37*, 533–541. [CrossRef]
11. Provis, J.L.; Bernal, S.A. Geopolymers and Related Alkali-Activated Materials. *Annu. Rev. Mater. Res.* **2014**, *44*, 299–327. [CrossRef]
12. Yang, J.; Huang, J.; He, X.; Su, Y.; Oh, S.-K. Shrinkage Properties and Microstructure of High Volume Ultrafine Phosphorous Slag Blended Cement Mortars with Superabsorbent Polymer. *J. Build. Eng.* **2020**, *29*, 101121. [CrossRef]
13. Wang, L.; Huang, Y.; Zhao, F.; Huo, T.; Chen, E.; Tang, S. Comparison between the Influence of Finely Ground Phosphorous Slag and Fly Ash on Frost Resistance, Pore Structures and Fractal Features of Hydraulic Concrete. *Fractal Fract.* **2022**, *6*, 598. [CrossRef]
14. Yong, C.L.; Mo, K.H.; Koting, S. Phosphorus Slag in Supplementary Cementitious and Alkali Activated Materials: A Review on Activation Methods. *Constr. Build. Mater.* **2022**, *352*, 129028. [CrossRef]
15. Yang, J.; Yu, X.; He, X.; Su, Y.; Zeng, J.; Dai, F.; Guan, S. Effect of Ultrafine Fly Ash and Water Glass Content on the Performance of Phosphorus Slag-Based Geopolymer. *Materials* **2022**, *15*, 5395. [CrossRef] [PubMed]
16. Klima, K.M.; Schollbach, K.; Brouwers, H.J.H.; Yu, Q. Thermal and fire resistance of Class F fly ash based geopolymers–A review. *Constr. Build. Mater.* **2022**, *323*, 126529. [CrossRef]
17. Chen, X.Y.; Klima, K.M.; Brouwers, H.J.H.; Yu, Q. Effect of silica aerogel on thermal insulation and acoustic absorption of geopolymer foam composites: The role of aerogel particle size. *Compos. Part B* **2022**, *242*, 110048. [CrossRef]
18. Babaee, M.; Castel, A. Water vapor sorption isotherms, pore structure, and moisture transport characteristics of alkali-activated and Portland cement-based binders. *Cem. Concr. Res.* **2018**, *113*, 99–120. [CrossRef]
19. Luo, Y.; Brouwers, H.J.H. Document details—Understanding the gel compatibility and thermal behavior of alkali activated Class F fly ash/ladle slag: The underlying role of Ca availability. *Cem. Concr. Res.* **2023**, *170*, 107198. [CrossRef]

20. Saleh, T.A. Protocols for Synthesis of Nanomaterials, Polymers, and Green Materials as Adsorbents for Water Treatment Technologies. *Environ. Technol. Innov.* **2021**, *24*, 101821. [CrossRef]
21. Czuma, N.; Panek, R.; Baran, P.; Zarębska, K. The Influence of Binders for the Pelletization of Fly Ash Zeolites on Sulfur Dioxide Sorption Properties. *Clay Miner.* **2020**, *55*, 40–47. [CrossRef]
22. Della Rocca, D.G.; Peralta, R.M.; Peralta, R.A.; Rodríguez-Castellón, E.; de Muniz Moreira, R.F.P. Adding Value to Aluminosilicate Solid Wastes to Produce Adsorbents, Catalysts and Filtration Membranes for Water and Wastewater Treatment. *J. Mater. Sci.* **2021**, *56*, 1039–1063. [CrossRef]
23. Minelli, M.; Medri, V.; Papa, E.; Miccio, F.; Landi, E.; Doghieri, F. Geopolymers as Solid Adsorbent for CO_2 Capture. *Chem. Eng. Sci.* **2016**, *148*, 267–274. [CrossRef]
24. Chai, W.S.; Cheun, J.Y.; Kumar, P.S.; Mubashir, M.; Majeed, Z.; Banat, F.; Ho, S.-H.; Show, P.L. A Review on Conventional and Novel Materials towards Heavy Metal Adsorption in Wastewater Treatment Application. *J. Clean. Prod.* **2021**, *296*, 126589. [CrossRef]
25. Global Energy Review: CO2 Emissions in 2021–Analysis. Available online: https://www.iea.org/reports/global-energy-review-co2-emissions-in-2021-2 (accessed on 25 October 2022).
26. Muhammad, B.; Khan, M.K. Foreign Direct Investment Inflow, Economic Growth, Energy Consumption, Globalization, and Carbon Dioxide Emission around the World. *Environ. Sci. Pollut. Res.* **2021**, *28*, 55643–55654. [CrossRef]
27. Quarterly Greenhouse Gas Emissions in the EU. Available online: https://ec.europa.eu/eurostat/statistics-explained/index.php?title=Quarterly_greenhouse_gas_emissions_in_the_EU (accessed on 26 October 2022).
28. KOBIZE. Available online: https://www.kobize.pl/ (accessed on 26 October 2022).
29. Czuma, N.; Franus, W.; Baran, P.; CWIK, A.; Zarębska, K. SO_2 Sorption Properties of Fly Ash Zeolites. *Turk. J. Chem.* **2020**, *44*, 155–167. [CrossRef] [PubMed]
30. Kim, J.; Lee, J.; Cho, H.; Ahn, Y. Life-Cycle Assessment of SO_2 Removal from Flue Gas Using Carbonate Melt. *J. Ind. Eng. Chem.* **2021**, *100*, 270–279. [CrossRef]
31. Hoesly, R.M.; Smith, S.J.; Feng, L.; Klimont, Z.; Janssens-Maenhout, G.; Pitkanen, T.; Seibert, J.J.; Vu, L.; Andres, R.J.; Bolt, R.M.; et al. Historical (1750–2014) Anthropogenic Emissions of Reactive Gases and Aerosols from the Community Emissions Data System (CEDS). *Geosci. Model Dev.* **2018**, *11*, 369–408. [CrossRef]
32. Xu, H.; Liang, W.; Xiang, K. The Environmental Consequences of Place-Based Policies in China: An Empirical Study Based on SO_2 Emission Data. *China World Econ.* **2022**, *30*, 201–229. [CrossRef]
33. EUR-Lex-Official Journal of the European Union. Available online: https://eur-lex.europa.eu/TodayOJ/ (accessed on 26 October 2022).
34. Garbalińska, H.; Cederholm, L. Przewodność cieplna betonu komórkowego różnych klas gęstości wyznaczana w różnym stanie zawilgocenia. *Mater. Bud.* **2019**, *1*, 58–61.
35. Zarębska, K.; Zabierowski, P.; Gazda-Grzywacz, M.; Czuma, N.; Baran, P. Fly Ash-Based Geopolymers with Refractoriness Properties. *Clean Technol. Environ. Policy* **2022**, *24*, 2161–2175. [CrossRef]
36. Brauneur, S.; Emmet, P.; Teller, E. Adsorption of Gases in Multi Molecular Layer. *J. Am Chem. Soc* **1938**, *60*, 309. [CrossRef]
37. Rouquerol, J.; Llewellyn, P.; Rouquerol, F. Is the BET Equation Applicable to Microporous Adsorbents. *Stud. Surf. Sci. Catal.* **2007**, *160*, 49–56.
38. Barrett, E.P.; Joyner, L.G.; Halenda, P.P. The Determination of Pore Volume and Area Distributions in Porous Substances. I. Computations from Nitrogen Isotherms. *J. Am. Chem. Soc.* **1951**, *73*, 373–380. [CrossRef]
39. Harkins, W.D.; Jura, G. An Adsorption Method for the Determination of the Area of a Solid without the Assumption of a Molecular Area, and the Area Occupied by Nitrogen Molecules on the Surfaces of Solids. *J. Chem. Phys.* **1943**, *11*, 431–432. [CrossRef]
40. Langmuir, I. The adsorption of gases on plane surfaces of glass, mica and platinum. *J. Am. Chem. Soc.* **1918**, *40*, 1361–1402. [CrossRef]
41. Beuchat, L.R.; Rockland, L.B. Influences of Hysteresis and Temperature on Moisture Sorption Isotherms. In *Water Activity*; Routledge: London, UK, 2017; pp. 173–213.
42. Anderson, R.B. Modification of the Brunauer, Emmett and Teller equations. *J. Am. Chem. Soc.* **1946**, *68*, 686–691. [CrossRef]
43. Guggenheim, E.A. *Application of Statistical Mechanics*; Clarendon Press: Oxford, UK, 1966.
44. De Boer, J.M. *The Dynamic Character of Adsorption*; Clarendon Press: Oxford, UK, 1953.

Disclaimer/Publisher's Note: The statements, opinions and data contained in all publications are solely those of the individual author(s) and contributor(s) and not of MDPI and/or the editor(s). MDPI and/or the editor(s) disclaim responsibility for any injury to people or property resulting from any ideas, methods, instructions or products referred to in the content.